1-2024

Leveraging High Resolution Classifications and Random Forests for Hindcasting Decades of Mesic Ecosystem Dynamics in the Landsat Time Series

N. E. Kolarik
Boise State University

N. Shrestha
Boise State University

T. Caughlin
Boise State University

J. S. Brandt
Boise State University

Publication Information

Kolarik, N. E.; Shrestha, N.; Caughlin, T.; and Brandt, J. S. (2024). "Leveraging High Resolution Classifications and Random Forests for Hindcasting Decades of Mesic Ecosystem Dynamics in the Landsat Time Series". *Ecological Indicators, 158*, 111445. https://doi.org/10.1016/j.ecolind.2023.111445

Ecological Indicators 158 (2024) 111445

Contents lists available at ScienceDirect

Ecological Indicators

journal homepage: www.elsevier.com/locate/ecolind

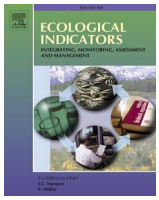

Leveraging high resolution classifications and random forests for hindcasting decades of mesic ecosystem dynamics in the Landsat time series

N.E. Kolarik [a,*], N. Shrestha [a], T. Caughlin [b], J.S. Brandt [a]

[a] Human Environment Systems, Boise State University, 1295 W University Dr, Boise, ID 83706, USA
[b] Department of Biological Sciences, Boise State University, 2133 W Cesar Chavez Ln, Boise, ID 83725, USA

ARTICLE INFO

Keywords:
Mesic ecosystems
Mesic vegetation
Semi-arid systems
Water resources
Restoration monitoring

ABSTRACT

Mesic ecosystems are fundamental to conservation efforts in semi-arid systems, but are threatened by climate change and development. Newer earth observation datasets, including Sentinel-1 and −2, provide opportunities to monitor mesic ecosystems at meaningful spatial scales, but are insufficient for measuring decadal-scale changes. Conversely, the Landsat time series has decades of data, but images are spatially coarse relative to many of the mesic ecosystem areas that sustain dryland systems, resulting in classifications with mixed pixels inadequate for effective monitoring. We developed a workflow that uses 10-m classifications produced from fusion of the Sentinel-1 and −2 time series (2017–2020) to estimate sub-pixel proportions of Landsat time series observations (2004–2020). Using random forest regression models, we quantified water resource proportions (WRP) of surface water, mesic vegetation, and upland land covers within each 30-m Landsat pixel. We incorporated ancillary covariates to account for varying topographic conditions, land cover, and climate. Results indicate that our approach consistently estimates sub-pixel proportions of Landsat pixels more accurately compared to spectral mixture analysis (SMA). The WRP product for surface water had up to 8% less error than SMA as measured by Mean Absolute Error (MAE) and up to 17% less error as measured by Root Mean Squared Error (RMSE). For mesic vegetation, the WRP product outperformed SMA by up to 4% (MAE) and 7% (RMSE). Finally, we demonstrated the ability of our time series to characterize historical water resource availability at a case study site with a well documented restoration history by qualitatively examining the mesic vegetation dynamics time series to identify system responses to restoration efforts. Our approach allows us to hindcast observations of Sentinel products and measure water resource dynamics with greater precision over larger temporal scales. We envision these WRP data to be useful for measuring the impacts of conservation interventions, disturbance recovery, or land use changes that pre-date the Sentinel time series.

1. Introduction

Water is essential to life and increasingly becoming more limited in dryland systems (Wang et al., 2023). Climatic uncertainty (Abatzoglou et al., 2017), population increases (Jones et al., 2019), land use change (Ahmed and Jackson-Smith, 2019), and irrigation strategies (Van Kirk et al., 2019) all contribute to reduced surface water, wetlands, and mesic meadows (hereafter water resources) across an already water limited landscape. The implications of uncertainty surrounding water resources for direct consumption and agriculture are of great concern to livelihoods in these systems globally. Ecosystem functions are also at risk as human development continues to encroach on relatively intact systems (Requena-Mullor et al., 2023). A spatially explicit understanding of the current extents and historical changes in water resources can help provide insight into sustainable paths of development and water resource allocation that minimize negative environmental impacts (Fig. 1).

Earth Observation (EO) data have been used extensively for mapping historical surface water dynamics via classification, particularly with the Landsat time series due to its open access and lengthy collection period (Feyisa et al., 2014; Gao, 1996; Pekel et al., 2016; Xu, 2006). However, dryland systems rely on relatively small surface water resource areas, such as small perennial and seasonal streams. In these systems, areas of mesic vegetation such as riparian zones, wetlands, and wet meadows indicate the presence of water but are spectrally quite different from surface water. Both surface water and mesic vegetation areas in semi-arid systems can remain undetected at the 30-m scale due to their

* Corresponding author.
E-mail address: nicholaskolarik@u.boisestate.edu (N.E. Kolarik).

https://doi.org/10.1016/j.ecolind.2023.111445
Received 25 September 2023; Received in revised form 10 December 2023; Accepted 14 December 2023
Available online 21 December 2023

small area relative to the pixels of the images used to measure them, resulting in mixed pixels. While the era of big data and cloud computing has ushered in efficient techniques for water resources monitoring (Donnelly et al., 2016; Pekel et al., 2016; Pickens et al., 2020), mixed pixels lead to incomplete inventories due to omission of smaller features. These omissions greatly limit our ability to monitor available water in systems where small water resource areas are integral to landscape functions.

Mesic vegetation and riparian vigor have received some attention from the EO community in recent years due to its importance as a resource area (Donnelly et al., 2016), for determining habitat quality (Hausner et al., 2018; Pilliod et al., 2021), and as an indicator of ecosystem resilience and function (Fairfax and Whittle, 2020). These studies typically rely on the normalized difference vegetation index (NDVI), which is a proven and easily calculable method for describing photosynthetic activity, and thus, overall vegetation and riparian health. However, using NDVI as an indicator of water availability in dryland systems has several limitations. First, NDVI can only describe vegetation vigor in a region of interest (Fairfax and Whittle, 2020; Pilliod et al., 2021; Silverman et al., 2019) and is not translatable to an area calculation without the use of a threshold or other classification technique. Second, when thresholding, using only NDVI typically requires the masking of large areas of forest vegetation (Donnelly et al., 2016), as dense conifer stands can have high photosynthetic activity, but lack mesic vegetation. In some forested settings, however, mesic vegetation resources are present (although to a lesser degree) and their dynamics have implications for landscape level functions (Barker et al., 2019). Lastly, in a mixed pixel containing both mesic vegetation and surface water, NDVI is reduced, therefore leading to conflicting signals as it relates to water availability (i.e. less surface water leads to higher NDVI values and vice versa).

To improve our ability to monitor water resources in dryland systems, there is a great need to quantify sub-pixel fractional coverage of both surface water and mesic vegetation among other land covers. Statistical spectral mixture analysis (SMA) (Bullock et al., 2020; Meyer and Okin, 2015) is historically the most common unmixing approach. In SMA, a model based on spectral properties of endmembers (pixels composed entirely of a single land cover class) estimates what proportion of each pixel is composed of each endmember. SMA has been effectively used in dryland systems to produce surface water estimates throughout the Landsat time series where each pixel in the modeled layer represents a fraction of water ranging from 0 to 100 % (Donnelly et al., 2019; Halabisky et al., 2016). A main advantage of SMA is that it requires only endmember spectral properties for parameterization. Furthermore, because SMA has been in use for a long time, built-in functions are easily accessible via image processing software. SMA

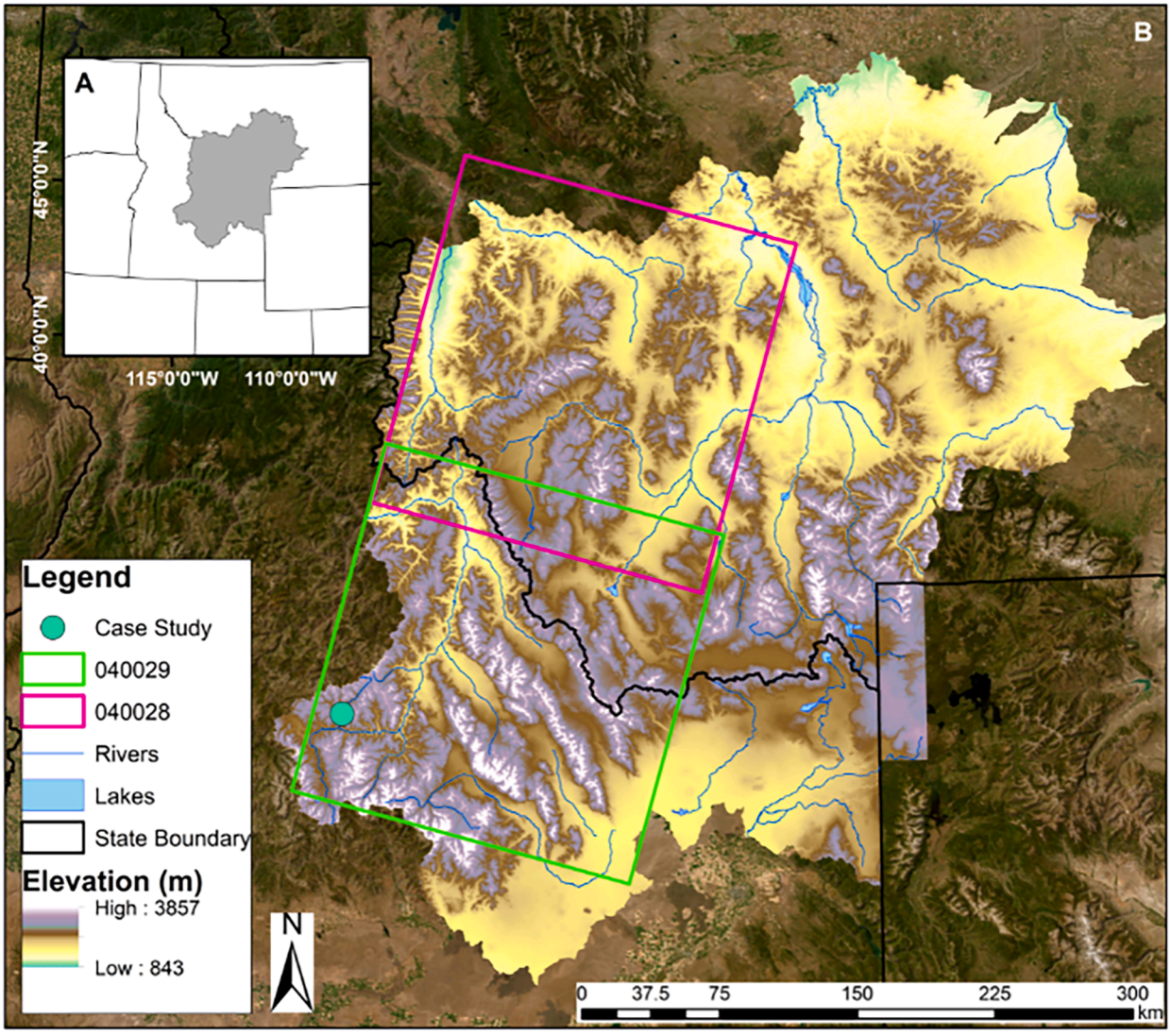

Fig. 1. Location of the High Divide, Landsat image footprints used, and the Yankee Fork case study site.

methods have shortcomings, however, as accessible methods depend heavily on the assumption that a linear relationship exists, where within-pixel reflectance values of other land cover categories may affect this assumption (Ray and Murray, 1996). Further, SMA accuracy and applicability is sensitive to the percent land cover present in any given pixel (Meyer and Okin, 2015), and the purity of endmembers selected (Deng and Wu, 2013).

Recently, nonparametric machine learning techniques have been increasingly employed for unmixing tasks (Okujeni et al., 2013; Rigge et al., 2020; Senf et al., 2020). Nonparametric machine learning approaches are data-driven rather than theory driven, and have shown to increase accuracy over statistical and probability based methods largely because they can account for the multiple scattering phenomenon known to affect the theoretical linear relationship (Yu et al., 2017). Machine learning methods not only show better prediction accuracy than traditional linear spectral unmixing methods, but are also capable of incorporating information beyond spectral reflectance to aid in prediction (Breiman, 2001; Huang et al., 2016). For example, ancillary covariates such as topography are key in distinguishing between spectrally similar, but ecologically important categories, like vegetation proportions in dryland systems (Rigge et al., 2020). We are unaware of any studies that have explored the utility of machine learning regressions for mapping water resources other than determining wetland likelihood (Reschke and Hüttich, 2014) and biomass estimation in wetlands (Mutanga et al., 2012), much less applying the models to a significant time-series.

One frequent barrier to the implementation of machine learning regression is that it requires a lot of training data that adequately cover the full possible outcome domain (Senf et al., 2020). Studies that have implemented machine learning approaches successfully have collected reference datasets in a variety of ways, including on the ground sampling, high resolution imagery, and hybrid methods (Rigge et al., 2020). However, the collection of adequate reference data is time consuming and expensive, and the most recent efforts use synthetically generated spectral mixtures to represent all possible land cover combinations (Okujeni et al., 2013; Senf et al., 2020; Stanimirova et al., 2022). Using synthetic spectral properties only, however, still results in errors among spectrally similar categories with important ecological and functional differences (Okujeni et al., 2013).

The Sentinel time series offers an alternative potential source for both land cover classification and training data, due to increased spatial and temporal resolution compared to Landsat (Du et al., 2016), but the time series is limited. The Sentinel constellation not only has optical sensors with bands comparable to Landsat (Sentinel 2a, 2b), but also a synthetic aperture radar (SAR) which can penetrate clouds and shown to be helpful for mapping water resources (Li and Niu, 2022; Mahdianpari et al., 2019; Slagter et al., 2020). With the first optical satellite (Sentinel-2A) launched in June 2015 and the second (Sentinel-2B) launched in March 2017, this limited time series alone is often insufficient for measuring longitudinal changes in water resource availability at 10 m spatial resolution. Sentinel classifications often fall short for measuring the influence of conservation initiatives and restoration projects due to their inability to capture before and after conditions necessary in observational studies in ecology (Seger et al., 2021). However, due to the amount of data available, Sentinel classifications could prove useful for estimating proportional coverage of Landsat scenes using machine learning regressions. While we are aware of studies that have hindcasted algal blooms (Ho et al., 2017), water quality (Deutsch and Alameddine, 2018) and crop yields (Evans and Shen, 2021) using in situ and climate data along with the Landsat time series, we are unaware of any hindcasting efforts using Landsat data trained with relatively high resolution classifications. Finding ways to incorporate Landsat images to hindcast products developed using the Sentinel time series is a possible solution to the tradeoff between spatial resolution and length of the collection period observed among these data sources.

The goal of this study is to better understand spatial and temporal dynamics of water resources in semi-arid landscapes affected by a changing climate and development. We focused our study in the semi-arid Intermountain Western US. Similar to many other regions across the globe, our study area is experiencing increased intensity and duration of drought, catastrophic wildfires, and population growth (Abatzoglou and Williams, 2016; Jones et al., 2019). Specifically, we used classifications developed in a previous study at the Sentinel spatial scale (10 m) (Kolarik et al., 2023) and ancillary covariates to estimate water resources proportions (WRP) within mixed pixels at the Landsat scale (30 m) in the overlapping temporal period (2017–2020) using scalable random forest regressions (Objective 1). We then applied these regressions to monthly Landsat composites from 2004 to 2016, with the aim of hindcasting water resources within mixed Landsat pixels as proportions throughout the time series and extending our classification time series backward to test whether our model performance holds outside of the temporal training domain (Objective 2). Using very high resolution images from the National Agricultural Imagery Program (NAIP), we assessed accuracy across heterogeneous landscape conditions, the training period, and hindcasted period to test whether the model appropriately captures system variability (Estes et al., 2018) (Objective 3). Using these WRP maps, we demonstrated the utility of our approach for describing water resource dynamics at a case study site with a documented restoration history (Objective 4).

2. Materials and methods

2.1. Study area

The High Divide, an area of Idaho and Montana that stretches between the Greater

Yellowstone Ecoregion and the Crown of the Continent is experiencing similar climatic challenges faced in drylands across the globe and much of the American West. These challenges contribute to reduced water availability across an already water limited landscape. The implications of uncertainty surrounding water resources for direct consumption and agriculture are of great concern to both agricultural and amenity based livelihoods (Dunham et al., 2018; Winkler et al., 2007). Further, ecosystem functions are at risk as human development continues to encroach on relatively intact ecosystems and the space between them.

2.2. Data inputs

2.2.1. Earth observation data

We accessed Landsat 8 Operational Land Imager (OLI) level two, collection two, tier one scenes across the study area in Google Earth Engine (GEE) from June to September for all years that overlap with the reliable Sentinel-2 time series (2017–2020) (Fig 2). We filtered the time series for images with less than 50 % cloud cover as indicated in the metadata, and applied the Fmask algorithm (Zhu et al., 2015) to remove remaining clouds and shadows and produce high-quality mosaics for each month. We then resampled these mosaics to align Landsat pixels to the Sentinel grid using a bilinear interpolation so that each Landsat pixel corresponds to nine Sentinel pixels. We conducted a sensitivity check for possible error introduced due to misregistration errors among Sentinel-2 and Landsat images. We added random noise with a standard deviation of 0.1 Landsat pixels following Skakun et al., (2017) to training and validation points and found little disagreement as demonstrated in Table S1, suggesting that these minor, sub-pixel level misregistrations contribute very little to error when these two rigorously orthorectified products in our study region. Beyond atmospherically corrected surface reflectance values, we also calculated normalized difference indices associated with water and greenness (NDWI, MNDWI, NDVI) (DeFries and Townshend, 1994; Gao, 1996; Xu, 2006).

To train the model to estimate proportions of water resources within each pixel of these monthly Landsat mosaics, we used 10 m monthly

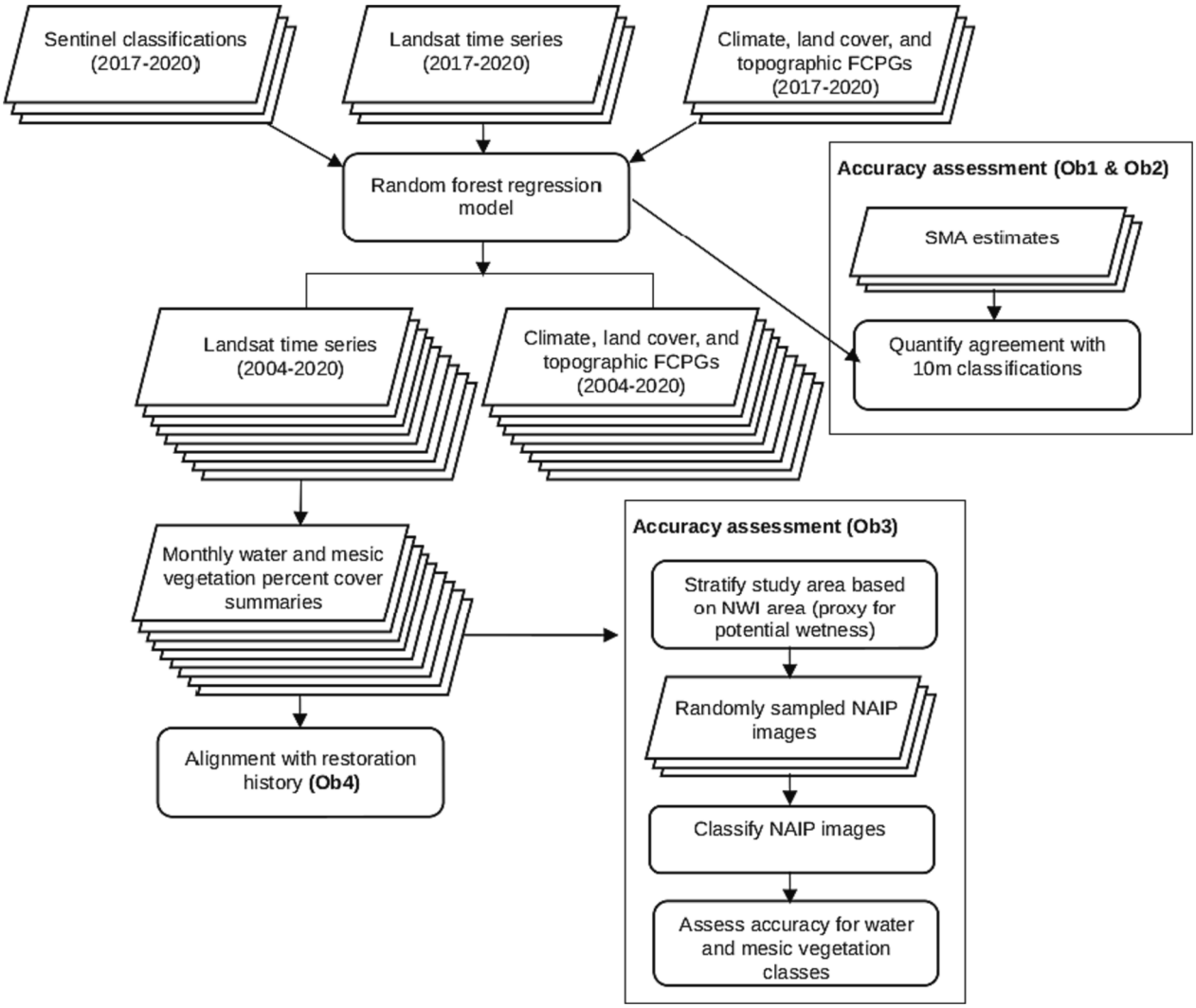

Fig. 2. Workflow diagram for generating water resources proportions (WRP) estimates, evaluating their accuracy, and a subsequent case study analysis.

classifications of water resources we produced in previous work (Kolarik et al., 2023). We produced these 10 m monthly water resource maps using a random forest classifier in a data fusion approach that incorporates optical and SAR Sentinel time series as well topographic variables. To do so, we leveraged the computing and storage resources of the GEE cloud environment to use all available SAR images, as well as all optical images with < 50 % cloud cover. We masked any remaining clouds in the optical images using the s2cloudless dataset. The maps we produced represent categories of open water, mesic vegetation, and other land covers (upland, shadow, and snow). We used every image available that met the quality criteria and used the monthly modes of the predominant land cover to label each pixel. Each Landsat pixel can be described as ninths of these three respective categories.

After training, we extended the model to level two, collection two, tier one images from Landsat 5, 7, and 8 and made monthly composites for the months of June-September from 2004 to 2016. Again, we masked clouds and applied transformations to Landsat 5 and 7 images following Roy et al. (2016) to account for spectral differences between Landsat missions.

2.2.2. *Ancillary data*

Rather than relying on spectral reflectance values alone for proportional estimates, we used topographic (hereafter time invariant), climatic, and land cover (hereafter time varying) variables to further constrain plausible quantities of water resources within each Landsat pixel (Table 1). Time invariant covariates included relatively simple topographic variables such as aspect, slope, and the topographic wetness index (TWI) shown to be helpful for identifying wetlands (Hird et al., 2017). We also use a wetland probability layer produced from SRTM and radar images (Hansen et al., 2021), which was helpful in our previous work for distinguishing shadows from water relative to the position on the landscape (Kolarik et al., 2023). Time varying covariates included climate variables such as temperature and precipitation values from PRISM (PRISM, n.d), as well as snow water equivalent data from the SNODAS archive (SNODAS, n.d). Further, we used MODIS evapotranspiration estimates to account for vegetation heterogeneity throughout the study area. We obtained land cover estimates for the contributing area using the National Land Cover Dataset (NLCD) (Homer and Fry, 2020). We focused on forest, wetland, and surface water as these are land covers shown to affect downstream water availability (Jaeger et al., 2019). Lastly, we estimated irrigated agriculture across the study area using the IrrMapper dataset (Ketchum et al., 2020), as we expect areas where upstream water resources are diverted to agriculture to realize lower wetness than a similar pixel with no withdrawals upstream. We incorporated time varying covariates using a flow conditioned parameter grid (FCPG) approach (Barnhart, 2020). This technique considers values of covariates for all contributing cells (utilizing a flow direction grid) and summarizes them as means. In doing so, the values in any given cell of the FCPG also reflect the contributing landscape rather than only local conditions. These considerations are logical, given that

Table 1
Covariates used in the random forest regression. *Italicized* text indicates FCPG covariates (time varying).

Covariate	Source
Blue	Landsat
Green	Landsat
Red	Landsat
NIR	Landsat
SWIR1	Landsat
SWIR2	Landsat
NDVI	Landsat
NDWI	Landsat
MNDWI	Landsat
Slope	SRTM
Aspect	SRTM
Elevation	SRTM
TWI	SRTM
Wetland Probability	Hansen et al., 2021
Irrigated Ag	*IrrMapper*
ET	*MODIS*
Precipitation	*PRISM*
March 1 SWE	*SNODAS*
May 1 SWE	*SNODAS*
Max temperature	*PRISM*
Min temperature	*PRISM*
Forest	*NLCD*
Surface Water	*NLCD*
Wetland	*NLCD*

precipitation in our study system falls predominantly as snow in the winter months and is released as the snow melts in spring and summer. To produce these FPCGs, we used the FCPGtools python package using TauDEM flow direction grids as documented by Barnhart (2020) on a high performance computing cluster.

2.3. Technical approach

2.3.1. Estimating proportions

2.3.1.1. Random forest regression. We use a random forest regression (RFR) approach to estimating proportions, where *n* decision trees are grown and data are split at nodes based on a random subset of covariates in each tree (Breiman, 2001). To perform these regressions, we use the built in random forest classifier function in GEE, with regression mode specified. We set the number of trees in the forest to 50, as increasing the size of the forest did not result in clearly stronger results, but came at a significant computational cost. We used the square root of the total number of covariates as the number of variables per split, a commonly used approach that reduces overfitting while providing strong results (Belgiu and Drăguţ, 2016).

We used the overlapping period of the Sentinel and Landsat time series (2017–2020) to train the RFR. We used six Landsat mosaics, three each from two different tiles (040029, 040028) in August 2017, July 2018, and September 2018, as these were the months where there were two Landsat images with less than 5 % cloud cover, resulting in nearly complete images with very few pixels contaminated by possible undetected clouds or cloud shadows. For each training image, we include the ancillary covariates for topographic variables using Terrain functions in GEE and the SRTM 30-m DEM and resampled the 10-m TWI layer used in Kolarik et al. (2023) to 30-m using the bilinear transformation method. We imported the FCPGs we produced for climate and land cover and included them in image stacks for each year (Table 1). Since land cover variables from the NLCD are not produced annually, we used the most recent year in each stack. We trained two models; one including the time varying covariates and the other without to test whether climatic and land cover/land use variation was adequately captured in spectral response or whether including these was absolutely necessary.

Due to the relatively small proportion of the landscape that contain water resources in our study system, we employed a stratified random sampling design to collect training samples for the RFR. For each category, we resampled binary outputs of the SF classification to 30-m resulting in fractional maps of a given land cover, with fractions ranging from zero to one in ninths. We then sampled 2,000 points from each of the ten possible values (0/9, 1/9, 2/9, etc.) from each image, resulting in 120,000 points for each class, 60,000 training points from each tile.

RFR and other machine learning regressions are constrained by their training data and will not predict a value outside of that domain. As a result, this approach is known to be biased high on the low end, and low on the high end (Belitz and Stackelberg, 2021). To resolve this bias, researchers have used several approaches, with the most common being a simple linear rotation (Huang et al., 2016; Stanimirova et al., 2022). However, we chose to use another RFR to estimate how the bias occurs relative to the covariates we used (Belitz and Stackelberg, 2021; Song, 2015), since this approach reduced bias more effectively in our application.

2.3.1.2. Spectral mixture analysis. For comparison with the RFR estimates, we conducted a more traditional linear spectral mixture analysis (SMA) previously used for monitoring water resources in the Western USA (Donnelly et al., 2019; Halabisky et al., 2016). We used the same training mosaics as outlined in the previous section. As endmembers, we used training points used for the RFR where all nine SF pixels were classified as either surface water, mesic vegetation, or other. Any differences in the outputs we then are able to attribute to the method used and covariates included for estimating proportions rather than the source of training. We used the unmix() function, the GEE version of a traditional linear spectral mixture analysis, where we also constrained the values to be non-negative and sum to one, with the goal of returning only realistic values.

2.3.2. Assessment

We conducted two accuracy assessments. First, we compared surface water and mesic vegetation estimates from both the WRP (RFR) and SMA to the Sentinel-based classifications. This assessment was conducted for the time period in which the WRP and Sentinel classifications overlapped (2017–2020). Second, we conducted a separate accuracy assessment using reference data derived from high resolution NAIP aerial photography. We define the resulting accuracies as the "absolute" accuracy. NAIP imagery is of high enough spatial resolution to represent on-the-ground conditions because even small water features are recognizable. Therefore, the "absolute" accuracy assessment enabled us to measure a) how well the WRP captures ground conditions of water availability, b) if there were differences in accuracy based on differences in environmental conditions (i.e. wetness of the landscape), and c) if the RFR was able to accurately "hindcast" water availability, i.e predict WRP in Landsat images that preceded the temporal domain of the input Sentinel classification training data.

2.3.2.1. Agreement with 10-m SF classifications. To assess the agreement between the WRP and the 10-m SF classifications from 2017 to 2020, we used monthly mosaics of the Landsat tile that overlaid our study area (040029) where there were two images in a month with less than 50 % cloud cover to reduce the likelihood of masked pixels. These months were August 2019, August 2020, and September 2020. For each model output, we stratified the validation sample in increments of 0.1, resulting in ten strata for each image. We sampled 100 points from each stratum, resulting in 1,000 validation points for each model output. We then calculated the mean absolute error (MAE) and root mean square error (RMSE) for each relative to the monthly maps we created at the 10-m scale using the SF classifier (Senf et al., 2020; Stanimirova et al., 2022). We calculated these for both the WRP and SMA estimates produced from Landsat images during the training period (2017–2020). We conducted these comparisons across the landscape as well as constrained

to low-lying locations where water resources are likely to occur, valley bottoms and flat slopes, as defined by the USGS Landforms dataset (Theobald et al., 2015).

2.3.2.2. Agreement with high resolution aerial images. For an absolute accuracy assessment of unmixed images, we randomly sampled images from the National Agricultural Imagery Program (NAIP). We stratified our study area using the National Wetlands Inventory (NWI) (NWI, 2023) as a guide to ensure the samples were representative of the range of possible mesic ecosystem conditions we seek to monitor (Pickens et al., 2020). The NWI represents a highly detailed inventory of surface water, riparian zones, and wetlands in the United States and is derived from highly detailed aerial photographs and field data. We laid a 20 km grid over the study area and created four (nearly) equal strata based on the area covered by all NWI categorized wetland types. The driest stratum ($n = 73$) ranged from blocks with < 1 % to 1.19 %, the dry stratum ($n = 74$) from 1.19 % to 1.91 %, the wet stratum ($n = 74$) from 1.91 % to 3.1 %, and the wettest stratum ($n = 73$) from 3.1 % to 32.6 % NWI wetland area. From each of these strata, we randomly selected ten blocks, and randomly selected a NAIP image from that block during the months of June through September from 2009 to 2020. We omitted images that did not fall completely within the image footprints that we regressed and/or have a corresponding monthly regression estimate due to our image selection criterion of < 50 % cloud cover. This resulted in only four images from the wettest stratum, and five images from each the wet and dry strata (Table S1). We chose not to include images from the driest stratum in our analysis due to the lack of water resources present.

Since false color images are only available from 2009 to present, we could not include all of the years we mapped into the sample pool. However, this period includes years that pre-date the Landsat 8 launch (2012), providing us the opportunity to assess maps we produced with images from Landsat 5 and 7 only. Since images in the wettest stratum were only sampled prior to the training period (Table S2), we omitted these from the analysis seeking to quantify differences in accuracy before and after the training period.

We then classified these high resolution NAIP images into classes of surface water, mesic vegetation, upland, shadow, and snow. For each image, we trained a random forest classification model by identifying training areas for each class in each image and continued to add more training data until the classifications appeared to be as high quality as possible (Pickens et al., 2020). The higher spatial resolution of these maps make them an ideal reference dataset for our coarser product (Olofsson et al., 2014). We resampled these classifications to 3-m and created binary maps of surface water/other and mesic vegetation/other, from which each Landsat pixel proportional estimate could be compared. From these, we created continuous cover maps at 30-m resolution for both surface water and mesic vegetation, where each pixel was described as a proportion of the given cover of interest. We then stacked these with the regressed outputs and produced 100 stratified random samples for each stratum in increments of 0.1 from each image, where available.

2.3.3. Case study analysis

To demonstrate the utility of the datasets we generated in this study, we applied our WRP times series to a restoration site with a detailed restoration history, the Yankee Fork of the Salmon River in Custer County, Idaho, USA. We worked with a stakeholder partner involved in the restoration at this site to reconstruct the restoration activities and water resource dynamics at the site. We delineated the site based on stakeholder knowledge and the historical floodplain, based on the USGS Landforms dataset (Theobald et al., 2015) areas described as either 'valley' or 'flat slope', as described in section 2.3.2.1. Within the case study site boundary, we calculated the proportion of the valley bottom occupied by mesic vegetation. The Yankee fork is an example of a main tributary where the stream channel of open water is narrow and/or covered by mesic vegetation, and thus we used mesic vegetation as the indicator of water availability. For reference, we also qualitatively analyzed the mesic vegetation dynamics in the context of the one year Standardized Precipitation Evapotranspiration Index (SPEI) (Abatzoglou, 2013) to assess whether changes were attributable to climatic fluctuation or restoration activities. For both, we used the loess function in base R (Shyu et al., 1992) to produce smoothed regressions of mesic vegetation and drought, respectively. We further calculated the area of mesic vegetation available before and after restoration. Since there is no consensus on how to estimate uncertainty in proportional coverage land change analyses (Stanimirova et al., 2022), we chose to follow the guidance of Stehman and Foody (2019) and use the mapped proportions of each fraction to produce weights for each fraction. We used the weights of each sampled fraction in NAIP classifications as outlined in section 2.3.2 (restricted to valley bottoms) to calculate a weighted standard deviation and construct 95 % confidence intervals ($z = 1.96$).

3. Results

3.1. Do water resources proportions (WRP) estimates in 30-m Landsat pixels from random forest regression accurately capture water resources compared to 10-m Sentinel classifications?

We found that the WRP compared well with surface water and mesic vegetation proportions characterized by Sentinel classifications. Further, we found no meaningful differences in the performance of the WRP model when we restrict the analyses to valley bottoms only. At the landscape scale, the MAE of proportions for surface water ranged from 0.19 to 0.20, and RMSE from 0.25 to 0.26 (Table 2). When restricted to valley bottoms only, the MAE range for surface water was identical (0.19 to 0.20), as was RMSE (0.25 to 0.26). The results for mesic vegetation were similarly consistent. The landscape scale MAE was 0.25 for all three images and the RMSE was 0.30. In valley bottoms only, MAE for mesic vegetation estimates ranged from 0.24 to 0.25 and RMSE ranged from 0.29 to 0.30.

3.2. Do random forest regressions capture water resource fractional coverage more accurately than spectral mixture analysis?

The SMA models based on the same training data were far less consistent than the WRP approach, particularly for surface water estimates (Table 2). In terms of MAE, we found the estimates to have consistently stronger agreement with the SF classifications when restricted to valley bottoms only. In fact, for the surface water class, the results show SMA has stronger or equal agreement with the reference classifications as the WRP model in terms of MAE, but always weaker agreement as measured by RMSE. With both metrics, mesic vegetation estimates were not as strong using the SMA approach as with the WRP. For surface water estimates, MAE ranged from 0.19 to 0.28 at the landscape level and RMSE from 0.31 to 0.43. However, when restricted to valley bottoms, MAE of surface water ranged only from 0.17 to 0.21, but RMSE from 0.28 to 0.33. MAE for mesic vegetation ranged from 0.29 to 0.30 and RMSE from 0.36 to 0.37 at the landscape level. When restricted to valley bottoms, mesic vegetation MAE ranged from 0.26 to 0.27 and RMSE from 0.34 to 0.35.

In Figs. 3 and 4, we show scatterplots that enable us to visualize errors across the entire range of the 0 to 100 % predictions in August 2019. In all plots, we see a much greater spread of values among SMA estimates when compared to WRP estimates (Figs. 3-4, Figs. S1-S4). For mesic vegetation specifically, densities are centered towards the middle of these distributions, regardless of the reference proportion. The SMA model routinely moderated the estimates further towards the middle range of possible proportions, resulting in less accurate estimates than with the WRP model.

In Figs. 5 and 6, we compare spatial differences between RFR and

Table 2
A comparison of accuracy metrics for SMA and RF regression (WRP) surface water and mesic vegetation proportional estimates. Negative differences for MAE and RMSE indicate stronger agreement with the reference among WRP estimates than SMA.

		WRP				SMA				Difference (WRP - SMA)			
		Water		Mesic		Water		Mesic		Water		Mesic	
		MAE	RMSE	MAE	RMSE	MAE	RMSE	MAE	RMSE	MAE	RMSE	MAE	RMSE
August 2019	Landscape	0.19	0.25	0.25	0.3	0.19	0.31	0.29	0.36	0	−0.06	−0.04	−0.06
	Valley Bottoms	0.19	0.25	0.24	0.3	0.17	0.28	0.26	0.34	0.02	−0.03	−0.02	−0.04
August 2020	Landscape	0.2	0.25	0.25	0.3	0.21	0.32	0.29	0.36	−0.01	−0.07	−0.04	−0.06
	Valley Bottoms	0.2	0.25	0.24	0.29	0.18	0.28	0.26	0.34	0.02	−0.03	−0.02	−0.05
September 2020	Landscape	0.2	0.26	0.25	0.3	0.28	0.43	0.3	0.37	−0.08	−0.17	−0.05	−0.07
	Valley Bottoms	0.2	0.26	0.25	0.29	0.2	0.33	0.27	0.35	0	−0.07	−0.02	−0.06

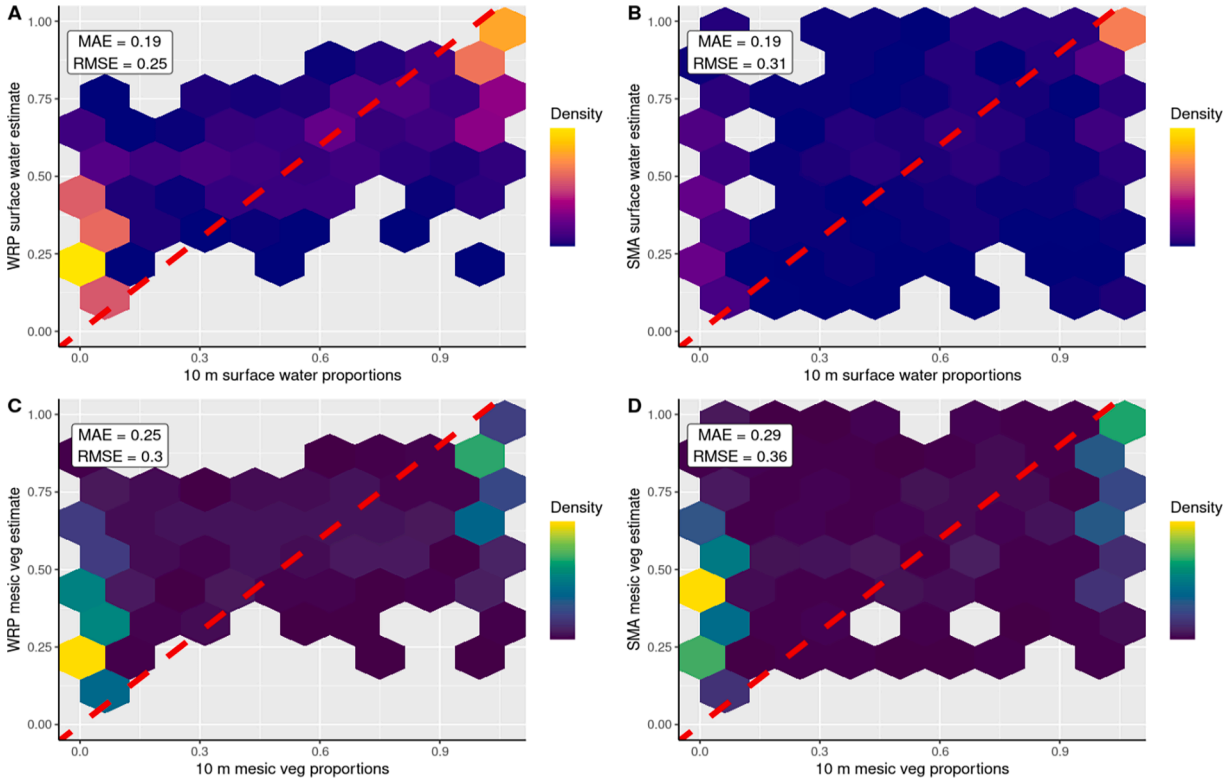

Fig. 3. August 2019 differences in agreement with the SF classifications of RF (A,C) and SMA (B,D) for surface water (A,B) and mesic vegetation (C,D). The red dashed lines represent 1:1 agreement.

SMA predictions, and include the National Wetlands Inventory (NWI) polygons as a reference of where likely wetland areas are located. We find that the SMA commits many more errors of commission in areas where surface water is not present (north facing slopes and densely forested areas), where the WRP estimates align more closely with the NWI polygons. The same is true for mesic vegetation estimates relative to the NWI areas.

For both surface water and mesic vegetation, we see a pattern of bias in the WRP estimates, despite applying a correction, where low values are estimated high, and high values estimated low, as seen in the scatter densities (Figs. 3 and 4; Figs. S1-S4). This pattern is apparent in the lake example of Fig. 6, where the WRP predicts that dense forests contain a non-zero proportion of mesic vegetation regardless of topographic position. Conversely, obvious lakes are predicted to have a non-zero fraction of mesic vegetation due to their topographic position. We see similar errors in SMA estimates, but with notably higher variance throughout, particularly in the middling ranges. While the SMA predicts an even higher fraction of mesic vegetation in dense forests due to reliance on spectral properties, it does not erroneously predict non-zero proportions of mesic vegetation in areas of open surface water within NWI polygons as does the RFR (Figs. 5-6).

Including time varying covariates did improve model performance consistently, but only by 0.01–0.02 for both MAE and RMSE in surface water and mesic vegetation proportional estimates (Table S3). The model without time varying covariates consistently outperformed the SMA models (Table S4), showing 0.04–0.12 proportional accuracy improvements for surface water at the landscape scale as measured by RMSE, and 0.02–0.05 in valley bottoms. Improvements in mesic vegetation proportions were less dependent on position relative to the valley bottom, with increases in proportional accuracy from 0.02 to 0.04 in MAE, and 0.04–0.07 in RMSE.

3.3. How accurate are fractional coverage estimates compared to "absolute" water resource conditions as measured from high resolution aerial photography?

Using the very high resolution NAIP classifications as reference revealed higher errors than when using the 10-m SF classifications, as is to be expected (Figs. S5-S7). We did find that agreement metrics were always stronger for surface water estimates than for mesic vegetation,

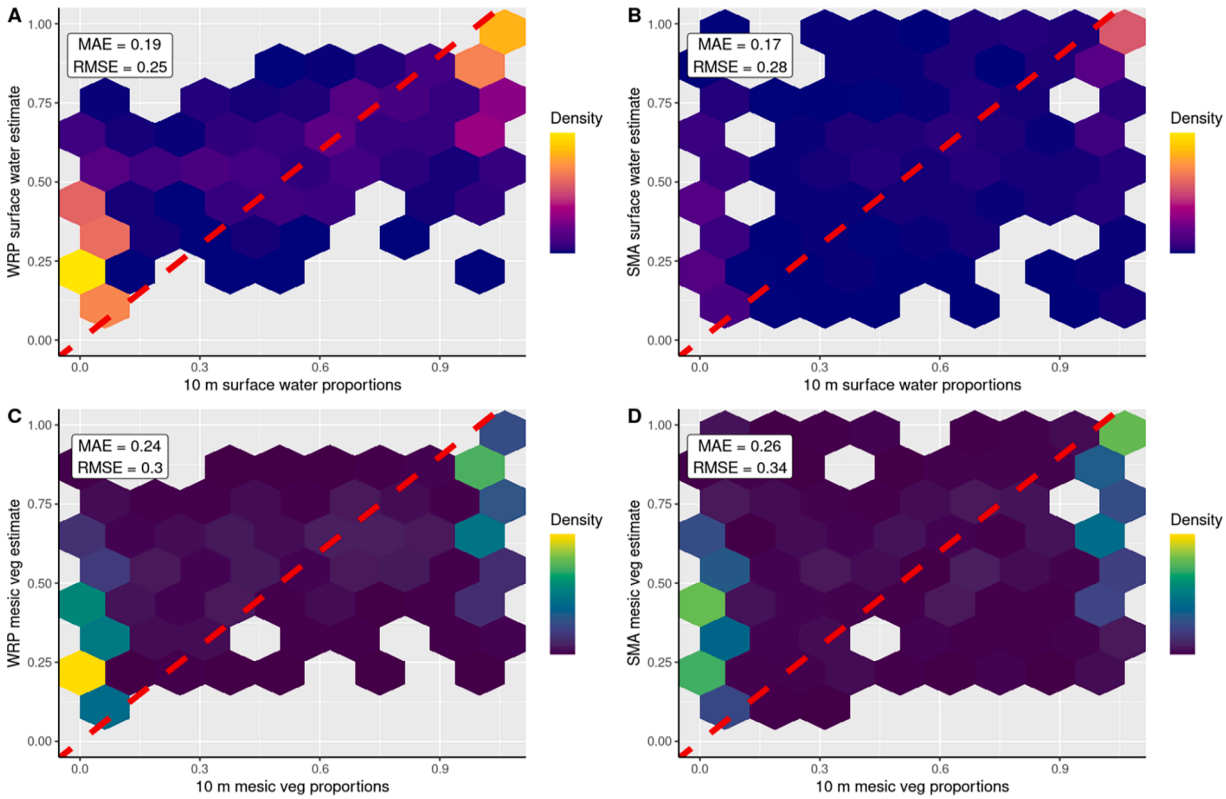

Fig. 4. August 2019 differences in agreement with the SF classifications of RF (A,C) and SMA (B,D) for surface water (A,B) and mesic vegetation (C,D) in valley bottoms only. The red dashed lines represent 1:1 agreement.

consistent with the previous analysis using 10-m classifications as reference. MAE for surface water ranged from 0.15 to 0.21 and RMSE from 0.19 to 0.26. For Mesic vegetation, MAE ranged from 0.30 to 0.36 and RMSE from 0.36 to 0.43 (Figs. S5-S7). Stratifying the study area using NWI area did not reveal any major differences relating to model performance, with variability relatively consistent regardless of the stratum analyzed.

When we aggregate the NAIP reference classifications based on their collection date relative to the training period (2017–2020), we do not see any meaningful differences. Error metrics indicate the WRP approach is robust, with MAE = 0.18 and RMSE = 0.22 before the training period (Fig. 7) and MAE = 0.18 and RMSE = 0.23 in the overlapping timeframe (Fig. 8). Agreement was slightly higher for the error metrics for mesic vegetation prior to the training period, with MAE = 0.32 and RMSE = 0.38 and MAE = 0.33 and RMSE = 0.40 during the training period. These results indicate that the WRP model is consistent, and the accuracy of estimates are not driven by image date relative to the training period.

3.4. Case study - change point detection at Yankee Fork of the Salmon River, Idaho, USA

Our historical reconstruction via stakeholder engagement illuminated a complex system with climatic variability and multiple interventions, which resulted in dramatic changes in water availability at the site. Like many riverscapes across the Western United States, the Yankee Fork was a highly degraded system and had lost many of its ecological functions due to alterations from the mining history in the area. From 1940 to 1952, 5.5 miles of this riverscape was dredged for gold extraction, pushing the river away from its functional state, into a degraded alternate stable state (Prettyman, 2020). Fluvial condition was highly altered, leaving little to no habitat for native salmonids, the channel was disconnected from its historic floodplain, and riparian vegetation almost absent (Colyer, 2021). Trout Unlimited (TU) partnered with government and tribal agencies to begin riverscape restoration in 2012. They removed dredge tailings, filled the ponds in the historical floodplain, converted them to side channels, installed an inlet control structure, and began planting riparian vegetation in the newly re-constructed floodplain. Riparian planting continued in 2013. In 2015, restoration interventions included the addition of unanchored trees to increase channel complexity, and large wood in the river to create micro-habitats for native salmonids (Casselle Wood; personal communication). These additions improved conditions enough that beavers returned to the area. In 2017, the reach experienced a 100 year flood event, which, along with the beaver activity and restoration interventions, spread water across the valley bottom during the early growing season, enhancing the growth of mesic vegetation at the site. As of 2023, beavers still inhabit the reach, and the hope of TU is that the project has created the conditions for them to remain there and maintain the ecosystem processes necessary for maintaining a healthy riverscape (Pollock et al., 2014).

When we plotted our WRP time series with major events from the historical reconstruction, we saw a response that fits well with the documented restoration history (Fig. 9). Vegetation extent dipped when the channel reconstruction occurred in 2012 at the beginning of restoration. In 2013, we observed a small rebound in mesic vegetation which coincided with riparian plantings. Mesic vegetation steadily increased from 2013 to 2020, a period in which the riparian plantings spread in the floodplain as a result of restoration interventions, beaver activity, and a major flood event. Specifically, floodplain vegetation continued to increase following the plantings and additions of woody debris in the channel, which was enough to attract beavers in 2015. Mesic vegetation in the floodplain continues to increase after the beavers established, an indication that the restoration successfully created enough deep pools and woody browse to maintain a beaver colony (Pollock et al., 2014). We also observe an increase in mesic vegetation that aligns with the

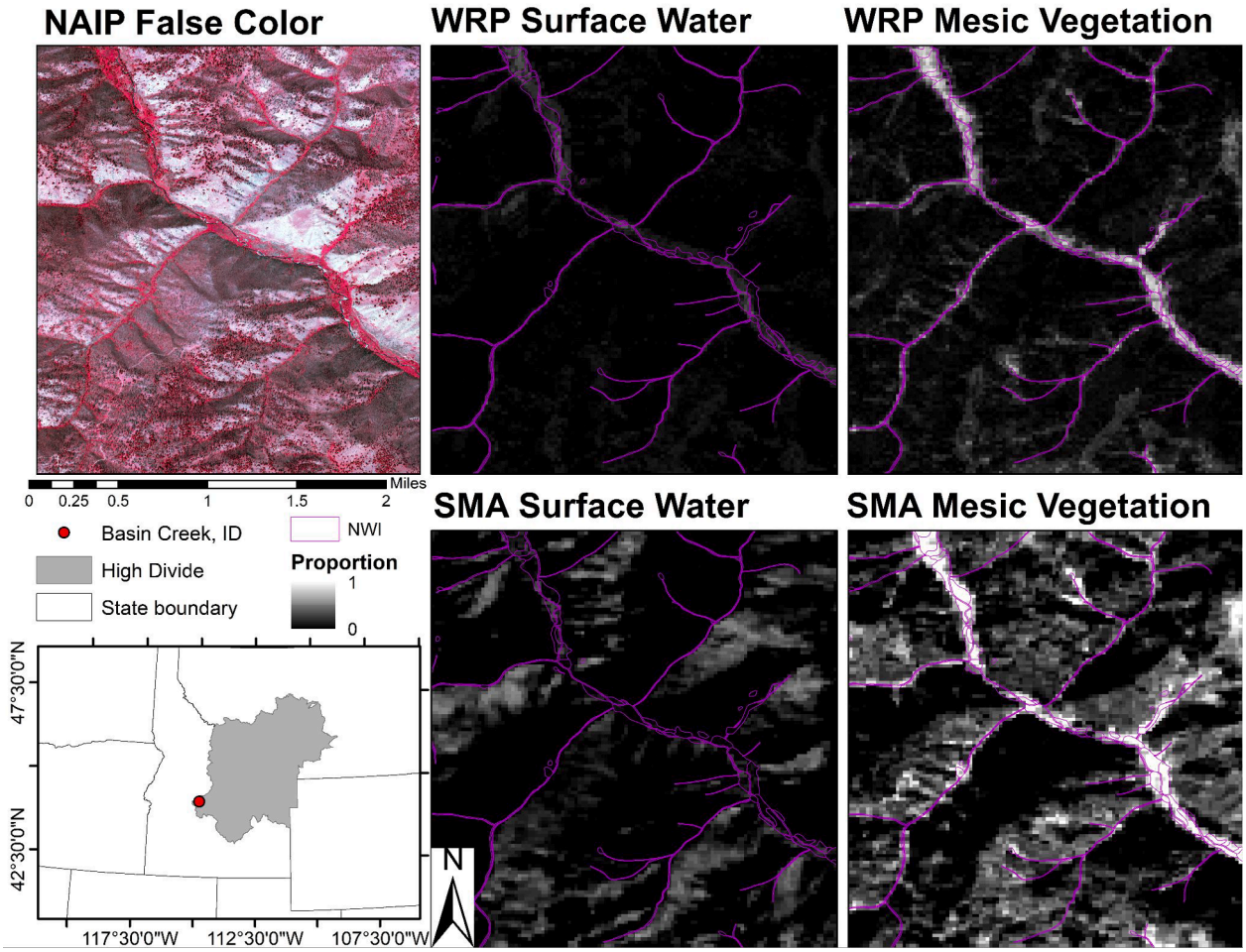

Fig. 5. A spatial comparison of the WRP estimates vs. SMA estimates in a riparian system.

2017 flood event. By the end of the time-series in 2020, the case study site established a new baseline mesic vegetation extent, near 46 % (+/- 29 %) of the valley bottom area, compared to 29 % (+/- 29 %) prior to the restoration. As converted to area, we estimate that mesic vegetation at this site has shifted from around 16,500 to 27,000 m^2 (+/- 17,246).

We also plotted the standardized precipitation evapotranspiration index (SPEI) values to qualitatively determine whether our mesic vegetation measures correspond to macro-level climate patterns. The SPEI indicates that there was a somewhat regular cycle/pattern of dry and wet years. Prior to restoration activity, mesic vegetation extent stayed relatively constant, despite climate variability, indicating that pre-restoration, the system seems to be in a stable state. However, since the start of restoration activities, we observe an increase in mesic vegetation, and the increases generally do not coincide with SPEI patterns, but the vegetation response is minimal in both of the potential alternate stable states we observe.

4. Discussion

Our results show that random forest regressions are a better choice for the mixed pixel problem regarding water resources in dryland systems than spectral mixture analysis. Our WRP product showed better agreement with the 10 m SF classifications than the SMA for both surface water and mesic vegetation for every validation image, and at both landscape and valley bottom scales as measured by RMSE. SMA can provide acceptable results where water resources are easily visible from above, and are in known locations, as has been shown to be effective in previous studies for monitoring surface water (Donnelly et al., 2019; Halabisky et al., 2016). However, the SMA routinely produced high outlying values. These outliers observed with the SMA approach could lead to unreliably high estimates of surface water, particularly in topographically complex environments where shadows are prevalent. In terms of mesic vegetation, estimates with the WRP approach are more reliable compared to than with SMA, regardless of spatial scale or location, leading to better resource inventories. This is important because mesic vegetation is a necessary indicator of landscape level water availability and key resources for terrestrial wildlife (Arkle and Pilliod, 2015; Barker et al., 2019; Donnelly et al., 2016; Kolarik et al., 2023).

We consider the observed increases in agreement to be attributable largely to the inclusion of time invariant topographic covariates found to be helpful in producing accurate classifications (Hird et al., 2017; Kolarik et al., 2023). These high level improvements, however, come at a cost as we allude to in the lake example. Including time invariant topographic covariates reduces errors in many cases, for instance for surface water in topographic shadows with a steep slope, or mesic vegetation in steep, densely forested areas. However, we suspect that these variables likely lead to smaller, but persistent commission errors in flat, low lying areas where both surface water and mesic vegetation are likely to occur, even if the spectral properties have conflicting information. In dryland systems, these errors are likely acceptable, given that areas where water resources could occur in these systems are so rare (Donnelly et al., 2016) and the trade-off of commission errors in relatively constrained valley bottoms versus vast upland areas is less consequential in the overall interpretation of the error and the maps.

An exciting finding of our study is that our model trained on

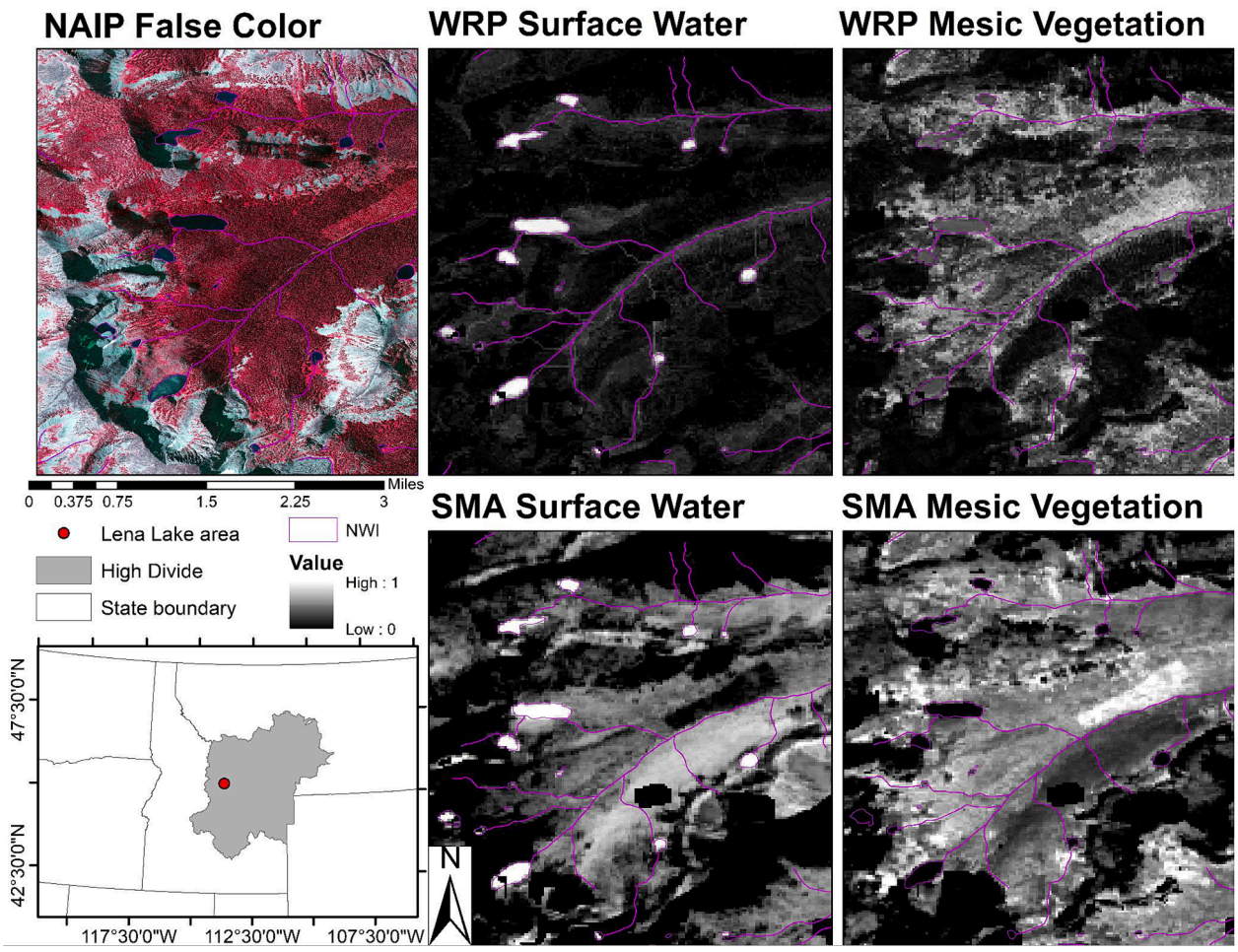

Fig. 6. A spatial comparison of the WRP estimates vs. SMA estimates in an alpine lake system. We include the National Wetlands Inventory (NWI) polygons for reference.

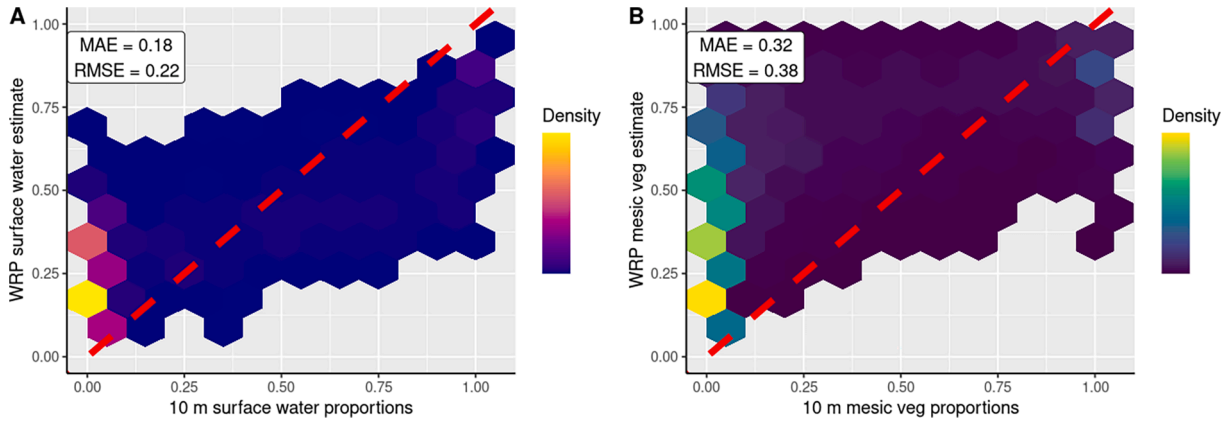

Fig. 7. Agreement with the NAIP classifications prior to the training period (2009–2016) for surface water (blue; A) and mesic vegetation (green; B). The red dashed lines represent 1:1 agreement.

relatively recent classifications can be used to accurately estimate proportions in pixels from past and future images, thus "extending" the temporal domains of higher resolution products. Thus, our approach captured enough variability in the observed ecological processes to produce reliable estimates beyond the temporal domain of the training data (Estes et al., 2018). The validation of hindcasted estimates is rare, as many hindcasting efforts only have data within the observation period (Deutsch and Alameddine, 2018; Evans and Shen, 2021; Ho et al., 2017), or use moderate to coarse remotely sensed data to validate their models (Chang et al., 2020; Ho et al., 2017).

We also show that higher resolution classifications can provide enough training data to train a random forest regression, in lieu of either costly reference data or synthetically generated training data. This approach is particularly effective when utilizing ancillary covariates such as climate and topography that can aid in differentiating spectrally similar, but ecologically important land covers. With the ubiquity of

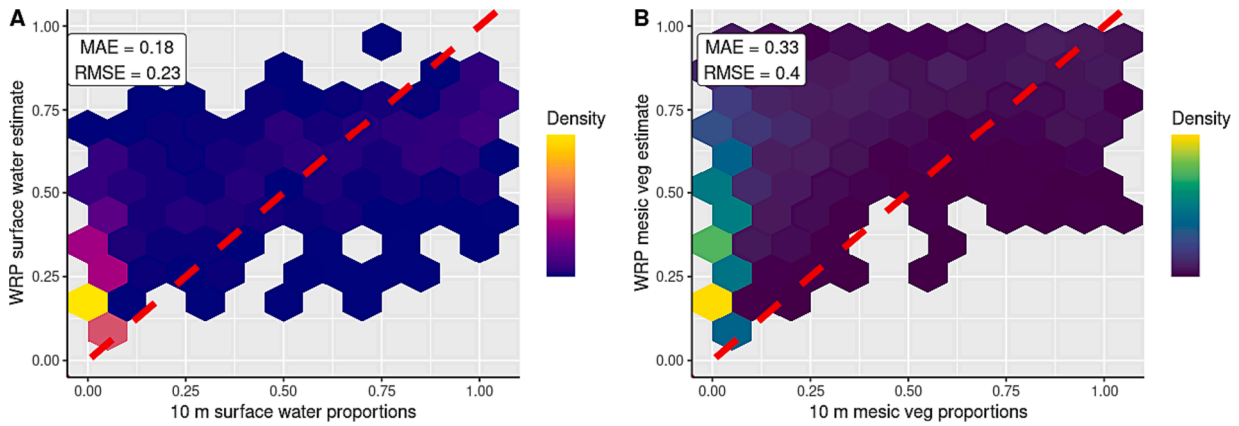

Fig. 8. Agreement with the NAIP classifications during the training period (2017–2020) for surface water (blue; A) and mesic vegetation (green; B). The red dashed lines represent 1:1 agreement.

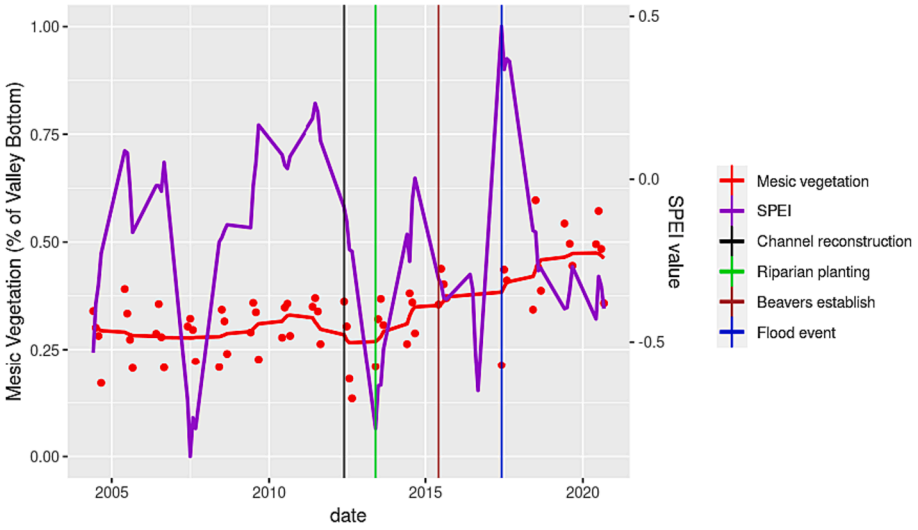

Fig. 9. Monthly time series of the proportion of mesic vegetation extent at the case study site. Key events are included for reference, as well as the one year SPEI values, where negative values indicate drier than normal conditions, and positive values indicate wetter than normal.

high-fidelity global datasets like the Dynamic World produced from Sentinel-2 images (Brown et al., 2022), to site specific unoccupied aerial systems applications (Carbonneau et al., 2020; Jochems et al., 2021; Linchant et al., 2015), the opportunity to extend the temporal record of classifications with very specific thematic resolutions could provide new opportunities to monitor habitat, invasive species, and natural resources.

We did not observe pronounced differences in WRP model performance based on strata. Surprisingly, the model performed similarly in the wettest and dry strata, but not as well in the wet stratum. This is counterintuitive given the results of recent work to update Canadian wetland inventories where the authors improved map accuracies by stratifying by ecoregion (Mahdianpari et al., 2020). We interpret our results as more of an indication of the quality of the image being unmixed (i.e. cloud cover, aerosols, or other contaminants) (Ho et al., 2017) rather than the amount of water resources found in a given location. It is likely that our study area, while heterogeneous in terms of vegetation cover, does not contain as starkly contrasting ecoregions as found in larger geographic areas.

Our hindcasted Landsat WRP time-series is capable of detecting meaningful changes in ecosystem conditions, as evidenced by our case study site analysis at a stream restoration site with a documented restoration history. The time series we examined matches well with in situ observations at the restoration site. One benefit of the WRP product is that we can estimate area of change, which is not possible with the more common approaches, like the normalized difference vegetation index (Fairfax and Small, 2018; Hausner et al., 2018). Our time series was able to detect changes in water availability that corresponded with management interventions (e.g. restoration activities), climatic events (e.g. a major flooding event), and ecological changes (e.g. the establishment of beaver). This analysis provides proof of concept of the applicability for land managers to incorporate scientific outputs into their monitoring routine, an often difficult, but important task for monitoring ecosystem recovery and developing sound management plans (Koontz, 2019). Important next steps include analyzing more case study sites in varying settings and locations, as well as using more rigorous statistical time-series techniques such as breakpoint and counterfactual analyses (Erdman and Emerson, 2008; Roopsind et al., 2019) to further identify the appropriate applications and limitations of our time series.

5. Caveats and limitations

We demonstrated that random forest regression outperforms spectral mixture analysis, but these improvements come at a computational cost, as incorporating ancillary covariates, particularly through the FCPG approach, requires more work on the front end and creates a more complex workflow than simply considering spectral and topographic

properties. We compared our WRP estimates with and without incorporating time varying climate and land cover FCPGs and found that WRP estimates with time varying covariates are more accurate than without but only minimally (1–2 %, Table S2). It is reasonable to expect that these covariates are captured in the spectral response, and incorporating time invariant topographic covariates along with spectral reflectance is enough to produce measurable improvements compared to SMA. While random forest regressions require more computing resources, generally, computing power has never been more accessible, particularly with cloud computing platforms like GEE that are easily accessible with a robust internet connection. Machine learning approaches and ancillary covariates should be routinely considered for unmixing tasks. Further accuracy improvements are likely if deep learning approaches would be considered (Shen et al., 2020), but these would require even more computational resources and are not freely available on the GEE platform.

We found the WRP estimates to be rather consistent across the validation images. A main concern here is the remaining biases of the model where low predictions are always biased high, and high predictions biased low resulting in a 'false moderation' effect among the estimates (Applestein and Germino, 2022; Belitz and Stackelberg, 2021). Despite the bias correction effort, the bias was not fully removed as also found in similar studies that utilize machine learning regression approaches (Stanimirova et al., 2022). This false moderation phenomenon is also observable in the SMA analyses, however, particularly for mesic vegetation. Though the false moderation effect results in samples that are biased towards the extremes of the value domain when using a stratified random sample, a simple random sample would have resulted in an extreme bias towards the low end of this domain given the relative scarcity of both surface water and mesic vegetation in the study area.

Our stratified sampling design for the assessment of the RFR model performance based on wetness as determined by the National Wetlands Inventory area revealed another issue. Images where errors were prevalent also had high forest cover, which complicates our analyses for several reasons. Shadows are more prevalent in NAIP images due to irregular acquisition times. There were many instances where shadows in the riparian zone made it impossible for us to label those areas otherwise. The RFR model will predict at least some proportion of water and mesic vegetation in these areas due to their topographic position. In these instances, there will always be disagreement, because we took a conservative approach when labeling these validation NAIP images that sometimes had longer light than would be desirable. Further, the RFR in these forested environments will predict at least some fraction of mesic vegetation due to the spectral response of the conifers (Breiman, 2001; Prasad et al., 2006).

A similar phenomenon arose in all images where there were very small creeks and streams. Even at 60 cm resolution, mixed pixels in these locations led to a classified value as either upland or shadow, and ultimately mislabeled pixels in the validation dataset. Without a suite of covariates beyond spectral properties, we cannot expect our approach of training a random forest classifier to produce a validation dataset to be exact in these areas. However, approaches where a grid of a given size is overlaid and an analyst describes each grid cell based on dominant cover (Stanimirova et al., 2022) also have disadvantages, as these provide less precision when trying to estimate proportions of ecologically meaningful, but often rare, categories like mesic vegetation.

Lastly, we should acknowledge that using discrete samples from a classification for training and validation is likely to propagate errors associated with creating discrete maps and products of continuous phenomena. For example, at the 10 m scale, mixed pixels remain prominent across the landscape particularly when dealing with small resource areas like surface water and mesic vegetation in dryland systems. Caution should always be used when interpreting maps or products that rely on discrete labels for mixed pixels. Further, despite using rigorously orthorectified images from popular and trustworthy data sources, misregistration of images can propagate errors into data products that also should be considered and evaluated (Barazzetti et al., 2016).

6. Conclusion

We demonstrate that using a machine learning approach, we can retrieve better estimates of surface water and mesic vegetation fractions in a mountainous semi-arid system than by using SMA. In doing so, we build on existing work for quantifying these relatively small resource areas that sustain semi-arid systems and their land functions. The maps we produce are useful for quantifying surface water and mesic vegetation changes as a result of restoration activities, disturbance events, or climate change. We consider this approach appropriate for extending the temporal record of high resolution classifications back in time, by using random forest regressions and the stalwart Landsat time series to estimate fractional coverage of ecologically important land covers. We posit that considering ancillary covariates such as topographic features, climatic and land cover conditions, along with spectral reflectance aids in estimating fractions of surface water and mesic vegetation in a given study area, and could be applicable to other resources and problems as well.

7. Funding statement

NASA FINESST Graduate student fellowship award (20-EARTH20-340). USDA NIFA Food and Agriculture Cyberinformatics and Tools (Grant #2739400), NASA Ecological Forecasting Applied Sciences (80NSSC 21K1353).

8. Code and data availability

https://code.earthengine.google.com/?accept_repo = users/nekolarik/SF_LS_MS.
https://github.com/neko1010/unmixingHD/tree/main

CRediT authorship contribution statement

N.E. Kolarik: Conceptualization, Data curation, Formal analysis, Funding acquisition, Investigation, Methodology, Software, Validation, Visualization, Writing – original draft, Writing – review & editing. **N. Shrestha:** Investigation, Methodology, Software, Validation, Writing – review & editing. **T. Caughlin:** Formal analysis, Investigation, Methodology, Supervision, Visualization, Writing – review & editing. **J.S. Brandt:** .

Declaration of competing interest

The authors declare that they have no known competing financial interests or personal relationships that could have appeared to influence the work reported in this paper.

Data availability

Data will be made available on request.

Appendix A. Supplementary data

Supplementary data to this article can be found online at https://doi.org/10.1016/j.ecolind.2023.111445.

References

Abatzoglou, J.T., 2013. Development of gridded surface meteorological data for ecological applications and modelling. Int. J. Climatol. 33, 121–131. https://doi.org/10.1002/joc.3413.

Abatzoglou, J.T., Williams, A.P., 2016. Impact of anthropogenic climate change on wildfire across western US forests. Proc. Natl. Acad. Sci. 113, 11770–11775. https://doi.org/10.1073/pnas.1607171113.
Abatzoglou, J.T., McEvoy, D.J., Redmond, K.T., 2017. The West Wide Drought Tracker: Drought Monitoring at Fine Spatial Scales. Bull. Am. Meteorol. Soc. 98, 1815–1820. https://doi.org/10.1175/BAMS-D-16-0193.1.
Ahmed, S., Jackson-Smith, D., 2019. Impacts of Spatial Patterns of Rural and Exurban Residential Development on Agricultural Trends in the Intermountain West. SAGE Open 9. https://doi.org/10.1177/2158244019871037.
Applestein, C., Germino, M.J., 2022. How do accuracy and model agreement vary with versioning, scale, and landscape heterogeneity for satellite-derived vegetation maps in sagebrush steppe? Ecol. Indic. 139, 108935 https://doi.org/10.1016/j.ecolind.2022.108935.
Arkle, R.S., Pilliod, D.S., 2015. Persistence at distributional edges: Columbia spotted frog habitat in the arid Great Basin, USA. Ecol. Evol. 5, 3704–3724. https://doi.org/10.1002/ece3.1627.
Barazzetti, L., Cuca, B., Previtali, M., 2016. Evaluation of registration accuracy between Sentinel-2 and Landsat 8, in: Fourth International Conference on Remote Sensing and Geoinformation of the Environment (RSCy2016). In: Presented at the Fourth International Conference on Remote Sensing and Geoinformation of the Environment (RSCy2016), pp. 71–79. https://doi.org/10.1117/12.2241765.
Barker, K.J., Mitchell, M.S., Proffitt, K.M., DeVoe, J.D., 2019. Land management alters traditional nutritional benefits of migration for elk. J. Wildl. Manag. 83, 167–174. https://doi.org/10.1002/jwmg.21564.
Barnhart, T.B., 2020. Flow-Conditioned Parameter Grids for the Contiguous United States: A Pilot. Seamless Basin Characteristic Dataset. https://doi.org/10.5066/P9HUWM6Q.
Belgiu, M., Drăguţ, L., 2016. Random forest in remote sensing: A review of applications and future directions. ISPRS J. Photogramm. Remote Sens. 114, 24–31. https://doi.org/10.1016/j.isprsjprs.2016.01.011.
Belitz, K., Stackelberg, P.E., 2021. Evaluation of six methods for correcting bias in estimates from ensemble tree machine learning regression models. Environ. Model. Softw. 139, 105006 https://doi.org/10.1016/j.envsoft.2021.105006.
Breiman, L., 2001. Random forests. Mach. Learn. 45, 5–32. https://doi.org/10.1023/A:1010933404324.
Brown, C.F., Brumby, S.P., Guzder-Williams, B., Birch, T., Hyde, S.B., Mazzariello, J., Czerwinski, W., Pasquarella, V.J., Haertel, R., Ilyushchenko, S., Schwehr, K., Weisse, M., Stolle, F., Hanson, C., Guinan, O., Moore, R., Tait, A.M., 2022. Dynamic World, Near real-time global 10 m land use land cover mapping. Sci. Data 9, 251. https://doi.org/10.1038/s41597-022-01307-4.
Bullock, E.L., Woodcock, C.E., Olofsson, P., 2020. Monitoring tropical forest degradation using spectral unmixing and Landsat time series analysis. Remote Sens. Environ. 238, 110968 https://doi.org/10.1016/j.rse.2018.11.011.
Carbonneau, P.E., Belletti, B., Micotti, M., Lastoria, B., Casaioli, M., Mariani, S., Marchetti, G., Bizzi, S., 2020. UAV-based training for fully fuzzy classification of Sentinel-2 fluvial scenes. Earth Surf. Process. Landf. esp.4955 https://doi.org/10.1002/esp.4955.
Chang, C.-H., Lee, H., Kim, D., Hwang, E., Hossain, F., Chishtie, F., Jayasinghe, S., Basnayake, S., 2020. Hindcast and forecast of daily inundation extents using satellite SAR and altimetry data with rotated empirical orthogonal function analysis: Case study in Tonle Sap Lake Floodplain. Remote Sens. Environ. 241, 111732 https://doi.org/10.1016/j.rse.2020.111732.
Colyer, W., 2021. Reflecting On The Yankee Fork Project - Trout Unlimited [WWW Document]. URL https://www.tu.org/magazine/conservation/reflecting-on-the-yankee-fork-project/ (accessed 4.17.23).
DeFries, R., Townshend, J.R.G., 1994. NDVI-derived land cover classifications at a global scale. Int. J. Remote Sens. 15, 3567–3586. https://doi.org/10.1080/01431169408954345.
Deng, C., Wu, C., 2013. The use of single-date MODIS imagery for estimating large-scale urban impervious surface fraction with spectral mixture analysis and machine learning techniques. ISPRS J. Photogramm. Remote Sens. 86, 100–110. https://doi.org/10.1016/j.isprsjprs.2013.09.010.
Deutsch, E.S., Alameddine, I., 2018. Hindcasting eutrophication and changes in temperature and storage volume in a semi-arid reservoir: a multi-decadal Landsat-based assessment. Environ. Monit. Assess. 191, 41. https://doi.org/10.1007/s10661-018-7180-7.
Donnelly, J.P., Naugle, D.E., Hagen, C.A., Maestas, J.D., 2016. Public lands and private waters: scarce mesic resources structure land tenure and sage-grouse distributions. Ecosphere 7, e01208.
Donnelly, J.P., Naugle, D.E., Collins, D.P., Dugger, B.D., Allred, B.W., Tack, J.D., Dreitz, V.J., 2019. Synchronizing conservation to seasonal wetland hydrology and waterbird migration in semi-arid landscapes. Ecosphere 10. https://doi.org/10.1002/ecs2.2758.
Du, Y., Zhang, Y., Ling, F., Wang, Q., Li, W., Li, X., 2016. Water bodies' mapping from sentinel-2 imagery with modified normalized difference water index at 10-m spatial resolution produced by sharpening the SWIR band. Remote Sens. 8, 354. https://doi.org/10.3390/rs8040354.
Dunham, J.B., Angermeier, P.L., Crausbay, S.D., Cravens, A.E., Gosnell, H., McEvoy, J., Moritz, M.A., Raheem, N., Sanford, T., 2018. Rivers are social–ecological systems: Time to integrate human dimensions into riverscape ecology and management. Wiley Interdiscip. Rev. Water 5, e1291.
Erdman, C., Emerson, J.W., 2008. bcp: An R Package for Performing a Bayesian Analysis of Change Point Problems. J. Stat. Softw. 23, 1–13. https://doi.org/10.18637/jss.v023.i03.
Estes, L., Elsen, P.R., Treuer, T., Ahmed, L., Caylor, K., Chang, J., Choi, J.J., Ellis, E.C., 2018. The spatial and temporal domains of modern ecology. Nat. Ecol. Evol. 2, 819–826. https://doi.org/10.1038/s41559-018-0524-4.
Evans, F.H., Shen, J., 2021. Long-term hindcasts of wheat yield in fields using remotely sensed phenology, climate data and machine learning. Remote Sens. 13, 2435. https://doi.org/10.3390/rs13132435.
Fairfax, E., Small, E.E., 2018. Using remote sensing to assess the impact of beaver damming on riparian evapotranspiration in an arid landscape. Ecohydrology 11, e1993.
Fairfax, E., Whittle, A., 2020. Smokey the Beaver: beaver-dammed riparian corridors stay green during wildfire throughout the western USA. Ecol. Appl. n/a, e2225.
Feyisa, G.L., Meilby, H., Fensholt, R., Proud, S.R., 2014. Automated Water Extraction Index: A new technique for surface water mapping using Landsat imagery. Remote Sens. Environ. 140, 23–35. https://doi.org/10.1016/j.rse.2013.08.029.
Gao, B., 1996. NDWI—A normalized difference water index for remote sensing of vegetation liquid water from space. Remote Sens. Environ. 58, 257–266. https://doi.org/10.1016/S0034-4257(96)00067-3.
Halabisky, M., Moskal, L.M., Gillespie, A., Hannam, M., 2016. Reconstructing semi-arid wetland surface water dynamics through spectral mixture analysis of a time series of Landsat satellite images (1984–2011). Remote Sens. Environ. 177, 171–183. https://doi.org/10.1016/j.rse.2016.02.040.
Hansen, M.C., Potapov, P.V., Pickens, A., Tyukavina, A., Hernandez Serna, A., Zalles, V., Turubanova, S., Kommareddy, I., Stehman, S.V., Song, X., Kommareddy, A., 2021. Global land use extent and dispersion within natural land cover using Landsat data. Environ. Res. Lett. https://doi.org/10.1088/1748-9326/ac46ec.
Hausner, M.B., Huntington, J.L., Nash, C., Morton, C., McEvoy, D.J., Pilliod, D.S., Hegewisch, K.C., Daudert, B., Abatzoglou, J.T., Grant, G., 2018. Assessing the effectiveness of riparian restoration projects using Landsat and precipitation data from the cloud-computing application ClimateEngine.org. Ecol. Eng. 120, 432–440. https://doi.org/10.1016/j.ecoleng.2018.06.024.
Hird, J.N., DeLancey, E.R., McDermid, G.J., Kariyeva, J., 2017. Google Earth Engine, Open-Access Satellite Data, and Machine Learning in Support of Large-Area Probabilistic Wetland Mapping. Remote Sens. 9, 1315. https://doi.org/10.3390/rs9121315.
Ho, J.C., Stumpf, R.P., Bridgeman, T.B., Michalak, A.M., 2017. Using Landsat to extend the historical record of lacustrine phytoplankton blooms: A Lake Erie case study. Remote Sens. Environ. 191, 273–285. https://doi.org/10.1016/j.rse.2016.12.013.
Homer, C., Fry, J., 2020. The National Land Cover Database. http://www.mrlc.gov/.
Huang, X., Schneider, A., Friedl, M.A., 2016. Mapping sub-pixel urban expansion in China using MODIS and DMSP/OLS nighttime lights. Remote Sens. Environ. 175, 92–108. https://doi.org/10.1016/j.rse.2015.12.042.
Jaeger, K.L., Sando, R., McShane, R.R., Dunham, J.B., Hockman-Wert, D.P., Kaiser, K.E., Hafen, K., Risley, J.C., Blasch, K.W., 2019. Probability of Streamflow Permanence Model (PROSPER): A spatially continuous model of annual streamflow permanence throughout the Pacific Northwest. J. Hydrol. X 2, 100005. https://doi.org/10.1016/j.hydroa.2018.100005.
Jochems, L.W., Brandt, J., Monks, A., Cattau, M., Kolarik, N., Tallant, J., Lishawa, S., 2021. Comparison of different analytical strategies for classifying invasive wetland vegetation in imagery from unpiloted aerial systems (UAS). Remote Sens. 13, 4733. https://doi.org/10.3390/rs13234733.
Jones, K., Abrams, J., Belote, R.T., Beltrán, B.J., Brandt, J., Carter, N., Castro, A.J., Chaffin, B.C., Metcalf, A.L., Roesch-McNally, G., Wallen, K.E., Williamson, M.A., 2019. The American West as a social-ecological region: drivers, dynamics and implications for nested social-ecological systems. Environ. Res. Lett. 14, 115008 https://doi.org/10.1088/1748-9326/ab4562.
Ketchum, D., Jencso, K., Maneta, M.P., Melton, F., Jones, M.O., Huntington, J., 2020. IrrMapper: A Machine Learning Approach for High Resolution Mapping of Irrigated Agriculture Across the Western U.S. Remote Sens. 12, 2328. https://doi.org/10.3390/rs12142328.
Kolarik, N.E., Roopsind, A., Pickens, A., Brandt, J.S., 2023. A satellite-based monitoring system for quantifying surface water and mesic vegetation dynamics in a semi-arid region. Ecol. Indic. 147, 109965 https://doi.org/10.1016/j.ecolind.2023.109965.
Koontz, T.M., 2019. The science-policy nexus in collaborative governance: use of science in ecosystem recovery planning. Rev. Policy Res. 36, 708–735. https://doi.org/10.1111/ropr.12362.
Li, Y., Niu, Z., 2022. Systematic method for mapping fine-resolution water cover types in China based on time series Sentinel-1 and 2 images. Int. J. Appl. Earth Obs. Geoinformation 106, 102656. https://doi.org/10.1016/j.jag.2021.102656.
Linchant, J., Lisein, J., Semeki, J., Lejeune, P., Vermeulen, C., 2015. Are unmanned aircraft systems (UASs) the future of wildlife monitoring? A review of accomplishments and challenges: A review of UASs in wildlife monitoring. Mammal Rev. 45, 239–252. https://doi.org/10.1111/mam.12046.
Mahdianpari, M., Salehi, B., Mohammadimanesh, F., Homayouni, S., Gill, E., 2019. The First Wetland Inventory Map of Newfoundland at a Spatial Resolution of 10 m Using Sentinel-1 and Sentinel-2 Data on the Google Earth Engine Cloud Computing Platform. Remote Sens. 11, 43. https://doi.org/10.3390/rs11010043.
Mahdianpari, M., Brisco, B., Granger, J.E., Mohammadimanesh, F., Salehi, B., Banks, S., Homayouni, S., Bourgeau-Chavez, L., Weng, Q., 2020. The Second Generation Canadian Wetland Inventory Map at 10 Meters Resolution Using Google Earth Engine. Can. J. Remote Sens. 46, 360–375. https://doi.org/10.1080/07038992.2020.1802584.
Meyer, T., Okin, G.S., 2015. Evaluation of spectral unmixing techniques using MODIS in a structurally complex savanna environment for retrieval of green vegetation, nonphotosynthetic vegetation, and soil fractional cover. Remote Sens. Environ. 161, 122–130. https://doi.org/10.1016/j.rse.2015.02.013.

Mutanga, O., Adam, E., Cho, M.A., 2012. High density biomass estimation for wetland vegetation using WorldView-2 imagery and random forest regression algorithm. Int. J. Appl. Earth Obs. Geoinformation 18, 399–406. https://doi.org/10.1016/j.jag.2012.03.012.

National Wetlands Inventory | U.S. Fish & Wildlife Service [WWW Document], 2023. URL https://www.fws.gov/program/national-wetlands-inventory (accessed 12.2.23).

Okujeni, A., van der Linden, S., Tits, L., Somers, B., Hostert, P., 2013. Support vector regression and synthetically mixed training data for quantifying urban land cover. Remote Sens. Environ. 137, 184–197. https://doi.org/10.1016/j.rse.2013.06.007.

Pekel, J.-F., Cottam, A., Gorelick, N., Belward, A.S., 2016. High-resolution mapping of global surface water and its long-term changes. Nature 540, 418–422. https://doi.org/10.1038/nature20584.

Pickens, A.H., Hansen, M.C., Hancher, M., Stehman, S.V., Tyukavina, A., Potapov, P., Marroquin, B., Sherani, Z., 2020. Mapping and sampling to characterize global inland water dynamics from 1999 to 2018 with full Landsat time-series. Remote Sens. Environ. 243, 111792 https://doi.org/10.1016/j.rse.2020.111792.

Pilliod, D.S., Hausner, M.B., Scherer, R.D., 2021. From satellites to frogs: Quantifying ecohydrological change, drought mitigation, and population demography in desert meadows. Sci. Total Environ. 758, 143632 https://doi.org/10.1016/j.scitotenv.2020.143632.

Pollock, M.M., Beechie, T.J., Wheaton, J.M., Jordan, C.E., Bouwes, N., Weber, N., Volk, C., 2014. Using Beaver Dams to Restore Incised Stream Ecosystems. BioScience 64, 279–290. https://doi.org/10.1093/biosci/biu036.

Prasad, A.M., Iverson, L.R., Liaw, A., 2006. Newer Classification and Regression Tree Techniques: Bagging and Random Forests for Ecological Prediction. Ecosystems 9, 181–199. https://doi.org/10.1007/s10021-005-0054-1.

Prettyman, B., 2020. Yankee Fork Fish Habitat Restoration Work Wrapping Up For 2020 - Trout Unlimited [WWW Document]. URL https://www.tu.org/press-releases/yankee-fork-fish-habitat-restoration-work-wrapping-up-for-2020/ (accessed 4.17.23).

PRISM Climate Group at Oregon State University [WWW Document], n.d. URL https://www.prism.oregonstate.edu/ (accessed 12.2.23).

Ray, T.W., Murray, B.C., 1996. Nonlinear spectral mixing in desert vegetation. Remote Sens. Environ. 55, 59–64. https://doi.org/10.1016/0034-4257(95)00171-9.

Requena-Mullor, J.M., Brandt, J., Williamson, M.A., Caughlin, T.T., 2023. Human population growth and accessibility from cities shape rangeland condition in the American West. Landsc. Urban Plan. 232, 104673 https://doi.org/10.1016/j.landurbplan.2022.104673.

Reschke, J., Hüttich, C., 2014. Continuous field mapping of Mediterranean wetlands using sub-pixel spectral signatures and multi-temporal Landsat data. Int. J. Appl. Earth Obs. Geoinformation 28, 220–229. https://doi.org/10.1016/j.jag.2013.12.014.

Rigge, M., Homer, C., Cleeves, L., Meyer, D.K., Bunde, B., Shi, H., Xian, G., Schell, S., Bobo, M., 2020. Quantifying Western U.S. Rangelands as Fractional Components with Multi-Resolution Remote Sensing and In Situ Data. Remote Sens. 12, 412. https://doi.org/10.3390/rs12030412.

Roopsind, A., Sohngen, B., Brandt, J., 2019. Evidence that a national REDD+ program reduces tree cover loss and carbon emissions in a high forest cover, low deforestation country. Proc. Natl. Acad. Sci. 116, 24492–24499. https://doi.org/10.1073/pnas.1904027116.

Roy, D.P., Kovalskyy, V., Zhang, H.K., Vermote, E.F., Yan, L., Kumar, S.S., Egorov, A., 2016. Characterization of Landsat-7 to Landsat-8 reflective wavelength and normalized difference vegetation index continuity. Remote Sens. Environ., Landsat Sci. Results 185, 57–70. https://doi.org/10.1016/j.rse.2015.12.024.

Seger, K.D., Sousa-Lima, R., Schmitter-Soto, J.J., Urban, E.R., 2021. Editorial: Before-After Control-Impact (BACI) Studies in the Ocean. Front. Mar. Sci. 8.

Senf, C., Laštovička, J., Okujeni, A., Heurich, M., van der Linden, S., 2020. A generalized regression-based unmixing model for mapping forest cover fractions throughout three decades of Landsat data. Remote Sens. Environ. 240, 111691 https://doi.org/10.1016/j.rse.2020.111691.

Shen, H., Jiang, Y., Li, T., Cheng, Q., Zeng, C., Zhang, L., 2020. Deep learning-based air temperature mapping by fusing remote sensing, station, simulation and socioeconomic data. Remote Sens. Environ. 240, 111692 https://doi.org/10.1016/j.rse.2020.111692.

Shyu, W.S.C., Eric Grosse, William M., 1992. Local Regression Models, in: Statistical Models in S. Routledge.

Silverman, N.L., Allred, B.W., Donnelly, J.P., Chapman, T.B., Maestas, J.D., Wheaton, J. M., White, J., Naugle, D.E., 2019. Low-tech riparian and wet meadow restoration increases vegetation productivity and resilience across semiarid rangelands: low-tech restoration increases vegetation productivity. Restor. Ecol. 27, 269–278. https://doi.org/10.1111/rec.12869.

Skakun, S., Roger, J.-C., Vermote, E.F., Masek, J.G., Justice, C.O., 2017. Automatic sub-pixel co-registration of Landsat-8 OLI and Sentinel-2A MSI images using phase correlation and machine learning based mapping. Int. J. Digit. Earth 10, 1253–1269. https://doi.org/10.1080/17538947.2017.1304586.

Slagter, B., Tsendbazar, N.-E., Vollrath, A., Reiche, J., 2020. Mapping wetland characteristics using temporally dense Sentinel-1 and Sentinel-2 data: A case study in the St. Lucia wetlands, South Africa. Int. J. Appl. Earth Obs. Geoinformation 86, 102009. https://doi.org/10.1016/j.jag.2019.102009.

Snow Data Assimilation System (SNODAS) Data Products at NSIDC, Version 1 [WWW Document], n.d. National Snow and Ice Data Center. URL https://nsidc.org/data/g02158/versions/1 (accessed 12.2.23).

Song, J., 2015. Bias corrections for Random Forest in regression using residual rotation. J. Korean Stat. Soc. 44, 321–326. https://doi.org/10.1016/j.jkss.2015.01.003.

Stanimirova, R., Graesser, J., Olofsson, P., Friedl, M.A., 2022. Widespread changes in 21st century vegetation cover in Argentina, Paraguay, and Uruguay. Remote Sens. Environ. 282, 113277 https://doi.org/10.1016/j.rse.2022.113277.

Stehman, S.V., Foody, G.M., 2019. Key issues in rigorous accuracy assessment of land cover products. Remote Sens. Environ. 231, 111199 https://doi.org/10.1016/j.rse.2019.05.018.

Theobald, D.M., Harrison-Atlas, D., Monahan, W.B., Albano, C.M., 2015. Ecologically-Relevant Maps of Landforms and Physiographic Diversity for Climate Adaptation Planning. PLOS ONE 10, e0143619.

Van Kirk, R., Hoffner, B., Verbeten, A., Yates, S., 2019. New approaches to providing instream flow for fisheries in the American West: Embracing prior appropriation and the marketplace, in: Multispecies and Watershed Approaches to Freshwater Fish Conservation; Dauwalter, DC, Birdsong, TW, Garret, GP, Eds. pp. 515–564.

Wang, H., Liu, Y., Wang, Y., Yao, Y., Wang, C., 2023. Land cover change in global drylands: A review. Sci. Total Environ. 863, 160943 https://doi.org/10.1016/j.scitotenv.2022.160943.

Winkler, R., Field, D.R., Luloff, A.E., Krannich, R.S., Williams, T., 2007. Social Landscapes of the Inter-Mountain West: A Comparison of 'Old West' and 'New West' Communities*. Rural Sociol. 72, 478–501. https://doi.org/10.1526/003601107781799281.

Xu, H., 2006. Modification of normalised difference water index (NDWI) to enhance open water features in remotely sensed imagery. Int. J. Remote Sens. 27, 3025–3033. https://doi.org/10.1080/01431160600589179.

Yu, J., Chen, D., Lin, Y., Ye, S., 2017. Comparison of linear and nonlinear spectral unmixing approaches: a case study with multispectral TM imagery. Int. J. Remote Sens. 38, 773–795. https://doi.org/10.1080/01431161.2016.1271475.

Zhu, Z., Wang, S., Woodcock, C.E., 2015. Improvement and expansion of the Fmask algorithm: cloud, cloud shadow, and snow detection for Landsats 4–7, 8, and Sentinel 2 images. Remote Sens. Environ. 159, 269–277. https://doi.org/10.1016/j.rse.2014.12.014.